IRAQI BULLETIN OF GEOLOGY AND MINING (IBGM)\
IRAQ GEOLOGICAL SURVEY (GEOSURV-IRAQ)

*IBGM (**2025**, Vol 21; Issue 1)* *15-38*

STRUCTURAL ANALYSIS AND MULTI-CRITERIA GIS-BASED LANDSLIDE SUSCEPTIBILITY MAPPING USING ANALYTICAL HIERARCHY PROCESS AND FREQUENCY RATIO MODEL, IN QAIWAN, GOIZHA, AZMER MOUNTAINS- NE IRAQ

Fahmy O. Mohammed[1], Salim H. Sulaiman Al-Hakari[1*], Ashna J. Ahmed[1], Sarkhel H. Mohammed[1,2]

[1] Department of Earth Science and Petroleum, College of Science, University of Sulaimani, Iraq
[2] Institute of Water Resources and Environmental Management, University of Miskolc, Hungary
***** *Corresponding author e-mail: salim.sulaiman@univsul.edu.iq*

Type of the Paper (Article)
Received: 27/ 04/ 2024
Accepted: 09/ 06/ 2024
Available online: 27/ 06/ 2025

Abstract

This study aimed to create a landslide susceptibility map for the Qaiwan, Goizha, and Azmer mountains series in northeastern Iraq, especially along the two-lane road network connecting the area to the Iranian border. The region holds significance for ecotourism within the Sulaimaniyah Governorate. Landslide susceptibility was assessed based on three methods. The first structural analysis of discontinuity reveals that the ac and bc set with hk0 > a, hk0 > b, and h0l > c systems are the most dominant discontinuity which acts as a back release and lateral release surfaces and causes the occurrence of different types of the landslide from more to less are wedge sliding, toppling, plane sliding, and rockfall. The second and third are landslide frequency ratio and analytical hierarchy process analyses which encompassing layers of slope, aspect, lithology, altitude, curvature, road network, and stream attributes were generated using remote sensing. These layers were integrated with ArcGIS software to create two maps, the first based on the analytical hierarchy process model and the second based on the landslide frequency ratio model. Landslide susceptibility maps were created and then classified into five zones: very low, low, moderate, high, and very high hazard. The moderate hazard zone covered the largest area (34.6 Km²), while the very high hazard zone was the smallest (5.5 Km²). The overall accuracy of the susceptibility map, assessed using appropriate methods, was approximately 75%, indicating the effectiveness of the employed models.

Keywords: Joint classification; Landslide hazard map; Susceptibility mapping; Accuracy assessment.

1. Introduction

Landslides are a prevalent geological phenomenon that has continuously drawn attention due to their destructive potential, causing significant harm to human settlements and infrastructure

ISSN 1811-4539, EISSN 3005-3714
https://doi.org/10.59150/ibgm2101a02
IBGM: http://ibgm-iq.org/
Academic Scientific Journals: www.iasj.net

(Tesfa, 2022). Landslides are complex processes influenced by multifaceted factors, including geological, geomorphological, and anthropogenic aspects (Das et al., 2012; Jaafari et al., 2014). Among these contributors, environmental factors, such as thawing slope, torrential rainfall, and surface topography variations play pivotal roles in triggering landslides (Choi et al., 2012). Understanding and predicting landslide susceptibility are imperative steps in mitigating their adverse effects and safeguarding vulnerable communities (Arjmandzadeh et al., 2020; F. O. Mohammed et al., 2020). Nonetheless, the complication of landslide causation, sometimes complex or unknown, causes significant challenges and needs detailed fieldwork and observation (Mamlesi, 2010). Geologic features and fractures, structural attributes, landforms, and vegetation cover also stand as primary contributors to landslide occurrences (Choi et al., 2012). Fractures analysis and landslide susceptibility mapping (LSM) stand as the cornerstone for decision-making, assisting citizens, planners, and engineers in minimizing losses caused by current and potential landslides through prevention, mitigation, and avoidance (Feizizadeh et al., 2014). Among the diverse methodologies available for LSM, the integration of multi-criteria decision analysis (MCDA) frequency ratio (FR) with geographic information systems (GIS) has emerged as a powerful tool (Abedini & Tulabi, 2018; Arjmandzadeh et al., 2020; Tesfa, 2022; Wu et al., 2016; Yalcin, 2008). The analytic hierarchy process (AHP), serving as an MCDA, systematically evaluates multiple criteria by assigning weights based on their relative importance. This approach forms a quantitative foundation for integrating diverse datasets, enabling a comprehensive analysis of landslide susceptibility factors (Achour et al., 2017; Basharat et al., 2016). The integration of AHP with GIS, known as MCDA, based on AHP (MCD-AHP), harnesses GIS's spatial capabilities to process and visualize intricate geospatial data.

The Qaiwan, Goizha, and Azmer Mountains region in northeast Iraq, with its rugged terrain and geological intricacies, stands as a challenging landscape susceptible to landslides (Al-Hakary, 2011; Hamasur & Qadir, 2020). Geological and structural conditions, land cover, slope steepness, and human activities are pivotal factors contributing to the region's susceptibility. Additionally, there are limited numbers of research that have been conducted in Qaiwan, Goizha, and Azmer dealing with landslide mapping.

This research endeavors to apply fracture analysis, and MCDA-AHP methodology alongside the FR model in the Qaiwan, Goizha, and Azmer Mountains regions of NE Iraq, aiming to elevate the precision and accuracy of LSM. By delving into the region's geological intricacies and systematically evaluating contributing factors, this study aims to contribute valuable insights to landslide research. Also based on the kinematics principle, which addresses the geometric requirements for the rock block to travel along the discontinuity plane different types of landslides were identified.

Finally, this research aims to provide practical tools for local authorities to mitigate landslides in the vulnerable Qaiwan, Goizha, and Azmer Mountains region and also offer insights to control landslide hazard risks in vulnerable areas this helps to minimize the impact of landslides on two-lane road network sides.

2. Study Area Description

The area of the research is located in the Qaiwan, Goizha, and Azmer Mountains in the northern and northeastern part of Sulaimani city, it is between coordinates Latitudes (35º34'45", 35º45'30") and Longitude (45º22'30", 45º32'00"; Figure 1). The elevation in the study area ranges between 900 – 1600 m with the slope ranges varying between <5° and >50°.

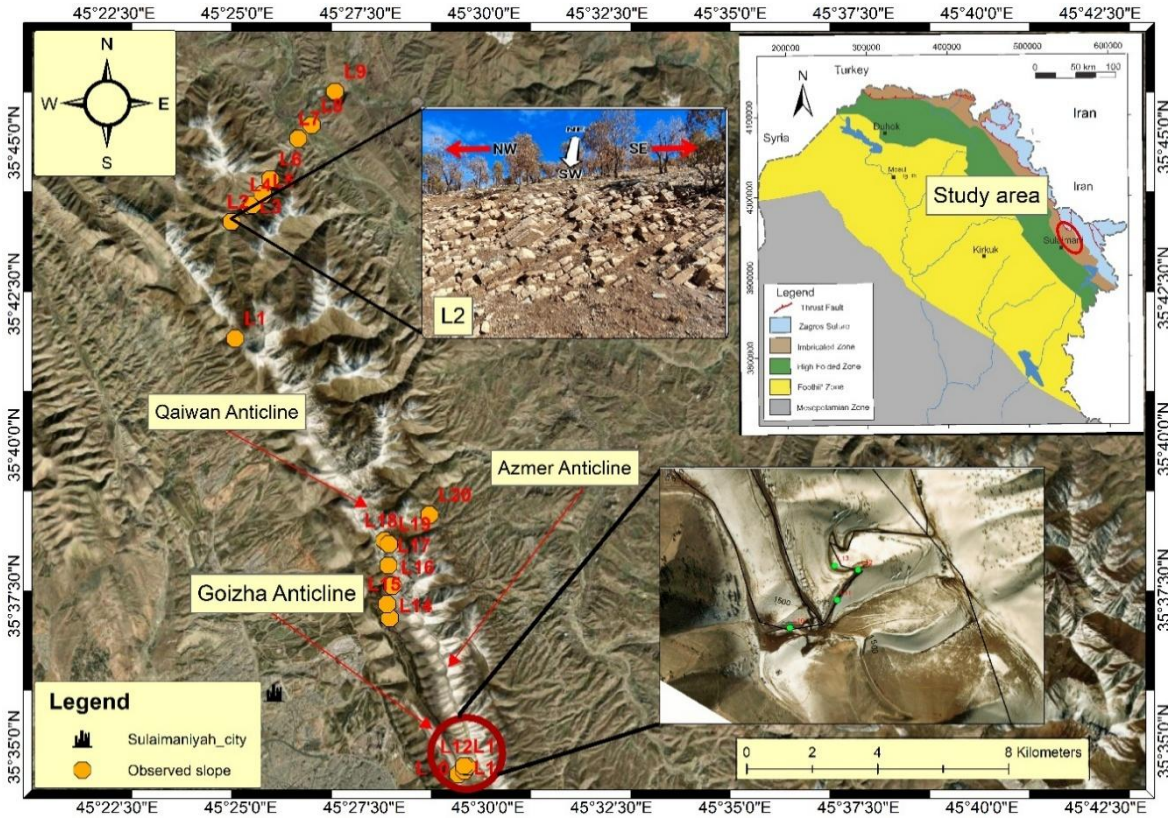

Figure 1. Location map of observed slopes and tectonic division of Iraq includes the location of the study area (The tectonic map after Fouad, 2015).

3. Geological Framework

The Qaiwan, Goizha, and Azmer Mountains are located at the boundary between high folded and imbricated zones of the Iraqi Zagros Fold Thrust Belt (Figure 1) It is characterized by long anticlines and narrow synclines. The outcropped rocks are highly fractured because the area is located within the high and imbricated tectonic zone of Iraq's tectonic subdivisions (Fouad, 2015; Mohammad, 2023). The trend of anticlines followed the Zagros Fold Thrust belt in the direction (NE – SW) with the SW fore limb (Alavi, 2007; Fouad, 2015). The main lithological units are from carbonate units of the Cretaceous periods which include Sarmord, Balambo, Kometan, Shiranish, and Aqra, formations from old to young (Buday, 1980; Jassim & Goff, 2006). Sarmord and Balambo formations are composed of highly jointed limestone and Marly limestone, the Kometan Formation is characterized by heavily jointed and fractured limestone with some chert nodules, the Shiranish Formation is composed of limestone, Marly limestone, and the Aqra Formation is composed of rudist rich limestone(Al-Hakary, 2011; Mohammad, 2023) (Figure 2).

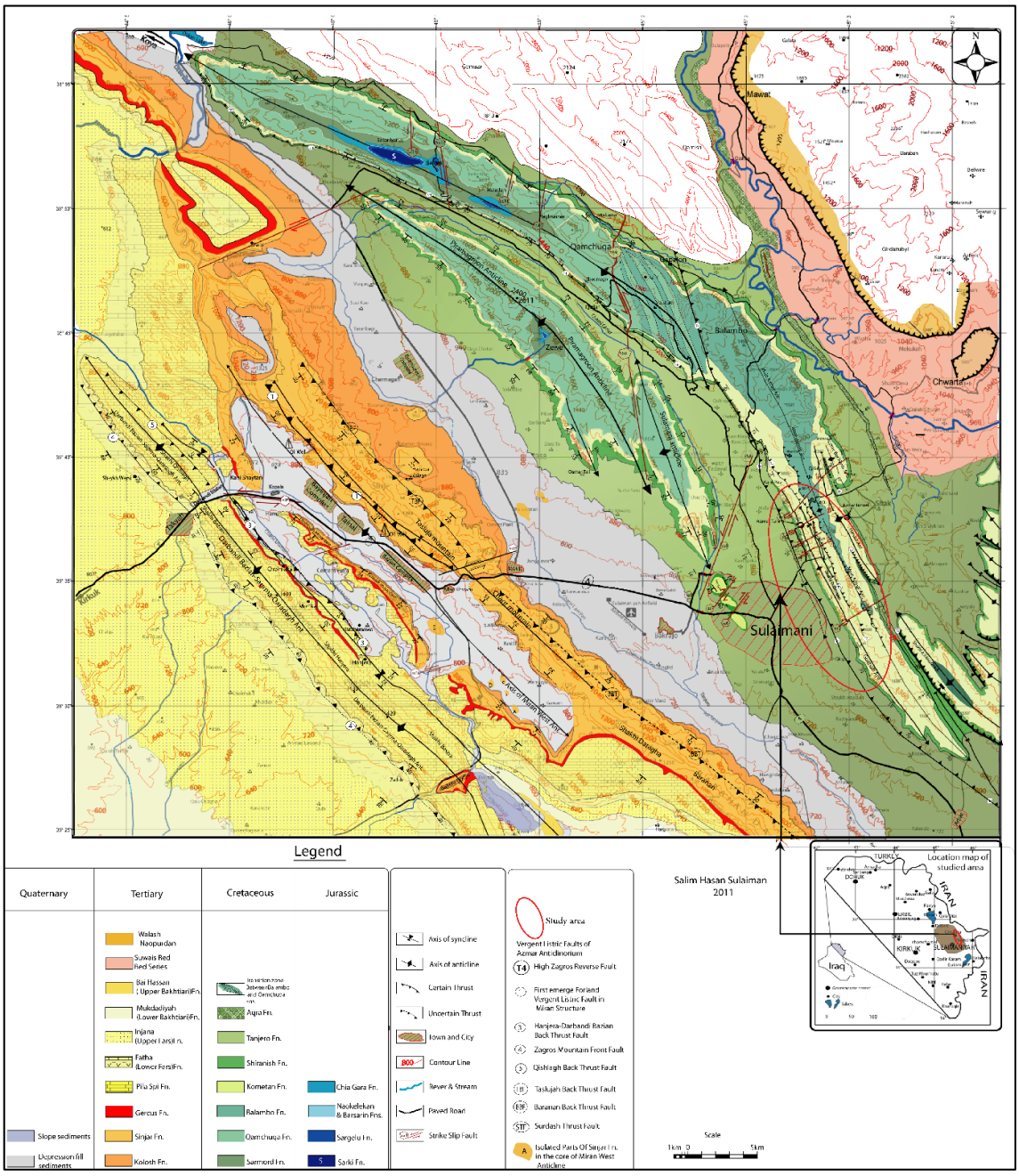

Figure 2. Geological map of the study area (Al-Hakary, 2011).

4. Material and Methods

The first step to compute the landslide susceptibility map was collecting data from the field during the winter and spring seasons of 2023 including selecting unstable slopes, discontinuity attitude measurements, and structural analysis of discontinuities followed by drawing thematic maps using remote sensing data, collecting ground truth data, weighted conventional maps in a GIS environment lead to drawing different raster maps such as slope, curvature, aspect, elevation, distance to road, distance to stream then the final map was creating use raster calculator (map algebra).

5. Structural Analysis of Discontinuities

To assess the structural factors (fractures and joints) affecting slope stability in the area, and control the different failure types in the study area, nine stations were chosen for data collecting (attitude of bedding plains and joints with inclination of the slops). Joints in the study area were classified according to their geometrical relations with the three perpendicular geometrical axes (a, b & c). Where (a) is parallel to the dip direction, (b) is parallel to the strike direction, and (c) is perpendicular to a & b. This classification is used by Turner & Weiss (1963) and followed by Al-Jumaily (2004), Hancock (1985), Hancock & Atiya (1979), and Ramsay et al. (1983) (Figure 3). Software DIPS 6.0 was used for constructing the data as pols for geometric classification (Figure 4).

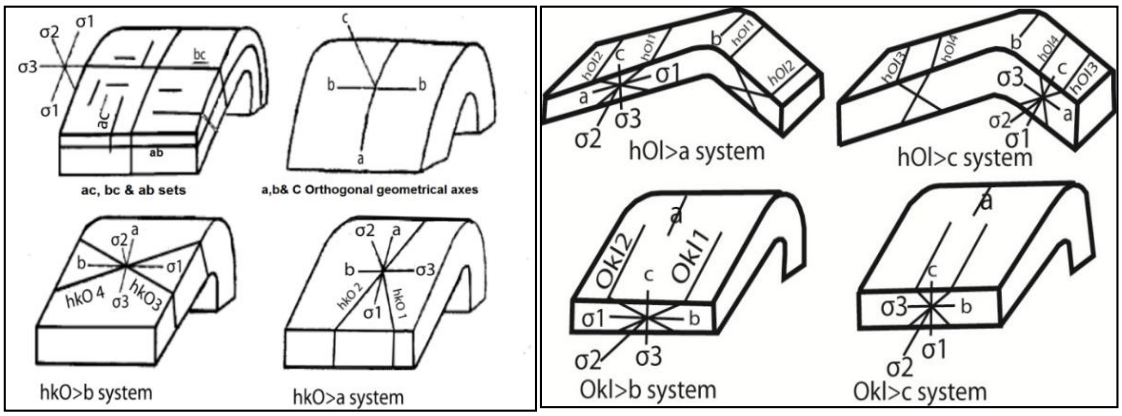

Figure 3. Geometrical classification of the joints with respect to three orthogonal geometrical axes (Hancock, 1985).

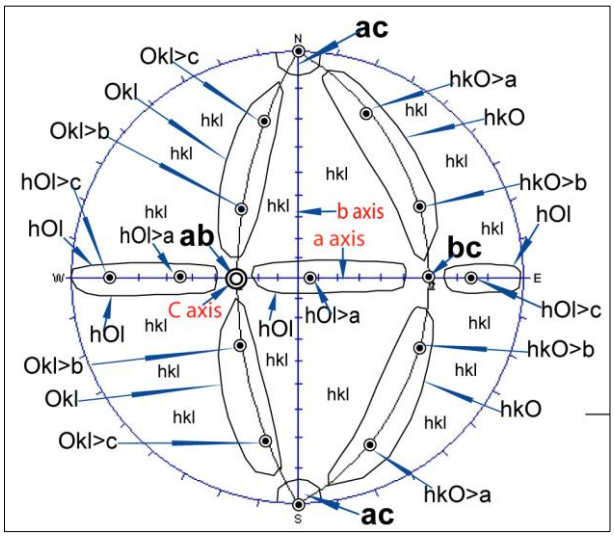

Figure 4. Classification of the joints based on their relations with the geometric axes a, b, and c by stereographic projection (Hancock and Atiya, 1979). The right great circle is the bedding plane its attitude is 180/30 (RHRL), and the left great circle is the perpendicular plane to the bedding plane. The figure shows the poles of all types of joints concerning the geometric axes a, b, and c.

6. Landslide Inventory Map

Landslide inventory mapping is the systematic mapping of existing landslides in the study area using different techniques, such as field surveys, aerial photographs, satellite image interpretation, and literature search for historical landslide records (Basharat et al., 2016; Tesfa, 2022). The landslide inventory map for our study area was compiled through the interpretation of satellite images Digital elevation model (DEM; 12.5 m × 12.5 m), and field-based inspection, it includes:

6.1. Slope (S)

Slope gradient plays a significant role in determining landslide susceptibility. Steeper slopes tend to be more prone to landslides due to gravitational forces. The steeper the slope, the greater the potential for instability and failure of the soil or rock mass. Water infiltration and soil saturation also increase with steep slopes, further elevating the risk of landslides (Saranaathan et al., 2021). The slope is a fundamental factor influencing LSM due to its direct correlation with gravitational forces. Steeper slopes are more prone to landslides because they have increased gravitational pull on the soil or rock mass. In GIS-based mapping, slope data can be derived from DEMs to categorize terrain into different slope classes (Figure 5A).

6.2. Curvature (C)

Curvature refers to the change in slope direction. Convex slopes (positive curvature) are more prone to landslides as they accumulate more water and materials. These areas often face greater erosion, leading to increased instability and higher susceptibility to landslides compared to concave slopes (negative curvature) (Lee & Pradhan, 2007). Conversely, negative curvature (concave slopes) might be less susceptible as they disperse water and materials, reducing the potential for landslide occurrence. Analyzing curvature data aids in identifying areas where convex slopes dominate, indicating a higher susceptibility to landslides (Figure 5B).

6.3. Aspect (A)

Aspect refers to the compass direction a slope faces. Landslide susceptibility varies based on aspect due to differential exposure to solar radiation, precipitation, and temperature changes. For instance, slopes facing certain directions might receive more sunlight or rainfall, affecting soil moisture content and consequently impacting landslides (Sarkar & Kanungo, 2004). GIS-based analysis involves categorizing aspects and assigning susceptibility values based on their orientation relative to external influences (Figure 5C).

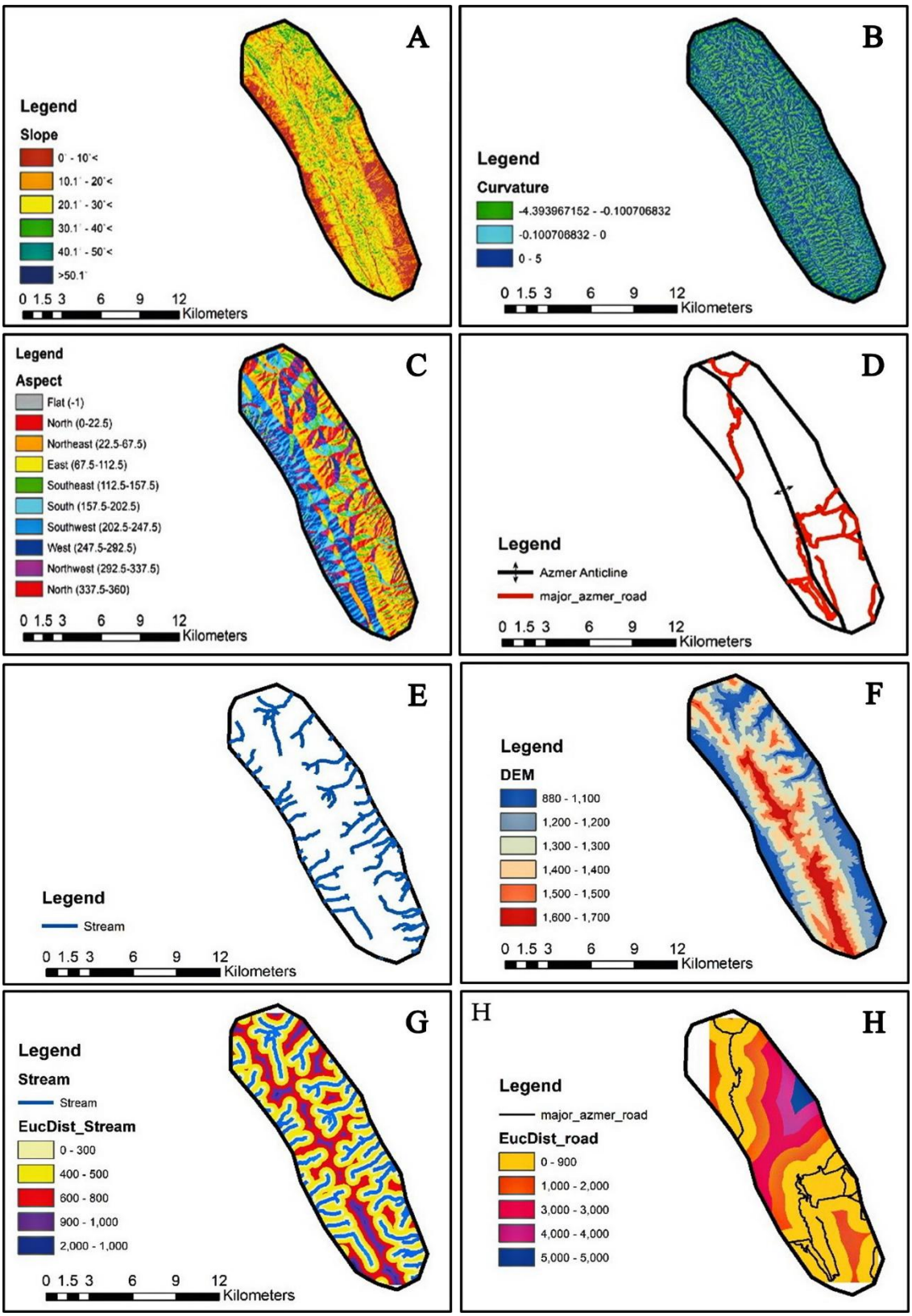

Figure 5. Thematic maps for the; (A) Slope, (B) Curvature, (C) Aspect, (D) Major road of the study area Thematic maps for the; (E) Stream, (F) Topography, (G) Euclidean distance to stream, and (H) Euclidean distance to road.

6.4. Distance to Road (DR)

Proximity to roads can influence landslide susceptibility. Roads can alter the natural drainage patterns and stability of slopes due to excavation, increased water runoff, and changes in slope angles caused by road construction activities. Moreover, road cuts can weaken adjacent slopes, making them more susceptible to landslides (El Jazouli et al., 2019). GIS-based mapping considers road proximity as a factor influencing susceptibility by assigning higher values to areas closer to roads due to increased human-induced disturbances and altered hydrological characteristics (Figure 5H).

6.5. Distance to Stream (DS)

Areas closer to streams or rivers are more vulnerable to landslides due to increased water content in the soil. The flow of water can erode and weaken slope materials, leading to instability and triggering landslides. Additionally, the force of flowing water can exert pressure on slopes, further increasing the likelihood of failure (Yalcin, 2008). GIS analysis involves delineating buffer zones around streams or rivers and assigning higher susceptibility values to areas within these zones (Figure 5G).

6.6. Topography (T)

Elevation influences landslide susceptibility by affecting various factors such as precipitation and geological characteristics. Higher elevations often receive more rainfall, leading to increased soil moisture content and erosion, which can enhance landslide susceptibility (Nefeslioglu et al., 2008). GIS-based mapping incorporates elevation data to categorize susceptibility zones, with higher elevations often being associated with increased susceptibility (Figure 5F).

6.7. Frequency ratio (FR) model

FR is a commonly used approach to mapping an LSM. It is a bivariate stochastic statistical method to assess the influence of various parameters on the occurrence of particular phenomena such as landslides (Lee et al., 2018). The FR model is implemented in a Geographic Information System (GIS) environment, making it easily applicable and interpretable. The approach of using historical landslide data to understand and predict future events is a widely employed strategy in landslide research, contributing valuable insights into the factors influencing slope stability by analyzing the correlation between past landslide locations and influencing factors. The FR method works to evaluate the relationships between different independent controlling factors that trigger the dependent factor which is landslide (Lee et al., 2018). A higher FR is followed by an intensive relationship between the occurrence of the possibility of the variables (Park et al., 2013).

The Landslide susceptibility index (LSI) is calculated using Equation 1.

$$LSI = \sum PFR, \quad (1)$$

Where LSI landslide Susceptibility index, FR is the frequency ratio.

The FR of each factor can be calculated using Equation 2.

$$PFR = \frac{\frac{P_{si}}{P_{Ni}}}{\frac{\sum_i^n P_{Fi}}{\sum_i^n P_{Ni}}}, \quad (2)$$

WWhere PFR: Is the probability frequency ratio, P_{si}: no. Number of pixels in Sub-Classes, P_{Ni}:

Total Number of pixels in class i, $\sum_i^n P_{Fi}$: Number of pixels in Factors, $\sum_i^n P_{Ni}$ Total number of pixels in the area.

$$LSZ = \sum_i^n PFR = SFR + AFR + CFR + DRFR + DSFR + TR, \quad (3)$$

Where LSZ = Landslide Susceptibility zones, SFR (slope frequency ratio), AFR (aspect frequency ratio, CFR (curvature frequency ratio), DRFR (distance to road frequency ratio), DSFR (distance to stream frequency ratio), and TRF (topography frequency ratio).

6.8. Analytical hierarchy process AHP

The AHP has emerged as a powerful methodology in the realm of LSM, offering a systematic and quantitative approach to evaluate and prioritize various influencing factors. Developed by Saaty (1980), the AHP methodology enables decision-makers to structure complex decision problems, facilitating the comparison and synthesis of diverse criteria. In LSM, AHP begins with the establishment of a hierarchy of criteria and sub-criteria relevant to the study area (T. L. Saaty et al., 2012), each criterion is then paired with every other criterion to derive pairwise comparison matrices. These pairwise comparisons are converted into a matrix, and the eigenvector method is employed to calculate the weights.

The calculated weights are then applied to the criteria, and their respective sub-criteria, to generate a comprehensive susceptibility index. AHP provides a robust framework for integrating qualitative and quantitative data, allowing for a comprehensive analysis of landslide susceptibility factors.

The consistency of judgments is assessed using the Consistency Ratio (CR), ensuring the reliability of the decision matrix where the result should have CR<0.1 to be consistent.

$$CR = \frac{CI}{RI} \quad (4)$$

Where CR: is the consistency ratio, CI is the consistency index, and RI is the random Index calculated by Saaty (2008) as shown in (Table 1) and (Table 2).

$$CI = \frac{\lambda max - n}{n - 1} \quad (5)$$

Where λmax is the maximum eigenvalue of the comparison matrix and n is the number of the matrix order.

$$LSI = Criteria1 \times Wc1 + Criterian \times Wcn, \quad (6)$$

Where W: Weightage from AHP, n: number of the criteria.

Table 1. Saaty's Score for the relative importance of criteria.

Scale	Relative Importance
1	Equality importance
3	Moderate Importance
5	Strong Importance
7	Very Strong Importance
9	Extreme Importance
2,4,6,8	Intermediate Value

Table 2. Calculated random index after (Wind & Saaty, 1980).

N	**1**	**2**	**3**	**4**	**5**	**6**
RI	0	0	0.58	0.90	1.12	1.2

7. Landslide Prone Area

To identify the most dangerous locations, field observations were conducted in the winter and spring of 2023. Twenty sites were chosen based on field observations; these sites are more likely to experience landslides and will provide a risk to vehicles, particularly in the winter when a rock falls and detached blocks may occur near the roadsides (Figure 6).

Figure 6. Some selected sites of Validations of models.

8. Results

8.1. Structural analysis

A detailed geometrical analysis of eight selected sites was done which reveals different lithologies and contains different types of rock failure types including wedge, toppling, plane sliding, and rockfalls as shown in (Figures 7, 8, and 9). Based on the geometrical classification of joints (Hancock & Atiya, 1979) the most prevalent joints that controlled unstable slope failures were ac and bc sets followed by hk0 > b, hk0 > a, h0l > c systems as shown in (Table 3). Also, the most dominant slope failure was wedging sliding, rockfall, toppling, and plane sliding, respectively as shown in (Table 4).

Table 3. discontinuity attitude in the study area.

	Geological Formation	**Slope /slope direction**		**Bedding plane Dip direction /Dip**	**Joint set (J1) Dip direction /Dip**	**Joint set (J2) Dip direction /Dip**
L2	Sarmord Fn.	255/58˚		035/48˚	275/61˚	178/50˚
L3	Balambo Fn.	199/60˚		239/44˚	133/74˚	057/74˚
L4	Balambo Fn.	191/54˚		239/44˚	141/85˚	047/52˚
L5	Balambo Fn.	170/60˚	SW limb (Left)	237/40˚	135/78˚	035/75˚
			NE limb (Right)	055/70˚	325/86˚	240/15˚
L6	Kometan Fn.	320/60˚	SW limb (Right)	038/54˚	310/83˚	235/35˚
			NE limb (Left)	270/40˚	135/55˚	035/68˚
L7	Kometan Fn.	267/52˚		253/42˚	130/62˚	075/46˚
L8	Shiranish Fn.	125/70˚		043/28˚	135/84˚	230/57˚
L9	Aqra Fn.	125/70˚		070/40˚	256/54˚	165/78˚

Table 4. Failure types in the study area.

Station	**Joint sets and systems**	**Slope failure types**
L2	hk0 > a system	Wedge and rockfall
L3	hk0 > a and h0l > c systems	Wedge, toppling, and rockfall
L4	ac and bc sets	Wedge and rockfall
L5 left (SW limb)	hk0 > a system	Wedge and rockfall
L5 right (NE limb)	ac and bc sets	Toppling
L6 left (SW limb)	0kl > b system	Wedge and rockfall
L6 right (NE limb)	ac and bc sets	Wedge and rockfall
L7	hk0 > b system and bc set	Plane sliding and rockfall
L8	ac and bc sets	Rockfall
L9	ac and bc sets	Plane sliding and rockfall

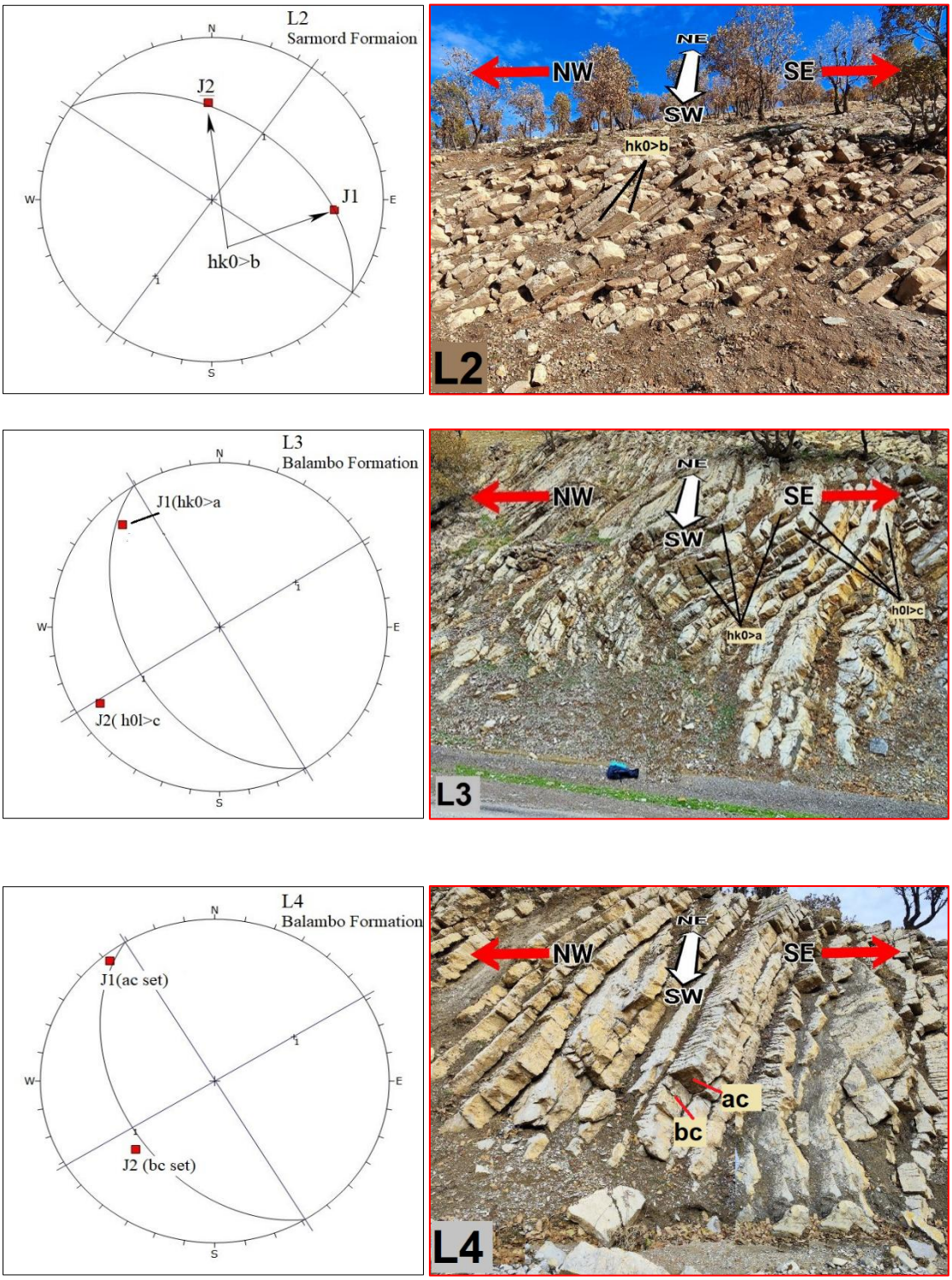

Figure 7. Shows stereographic projection of the joints and field photos of (L2, L3, and L4) stations.

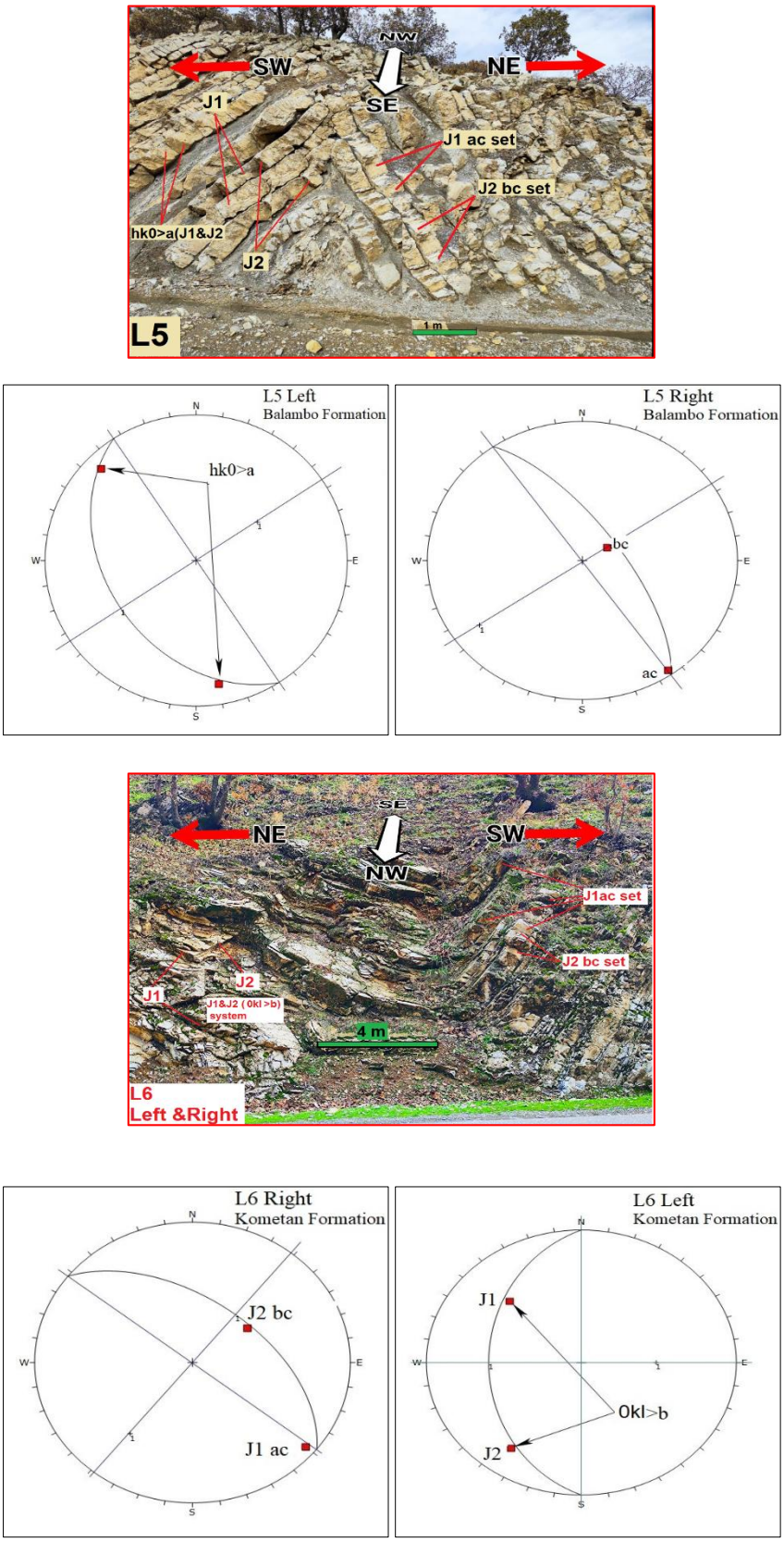

Figure 8. Shows stereographic projection of the joints and field photos of (L5 and L6).

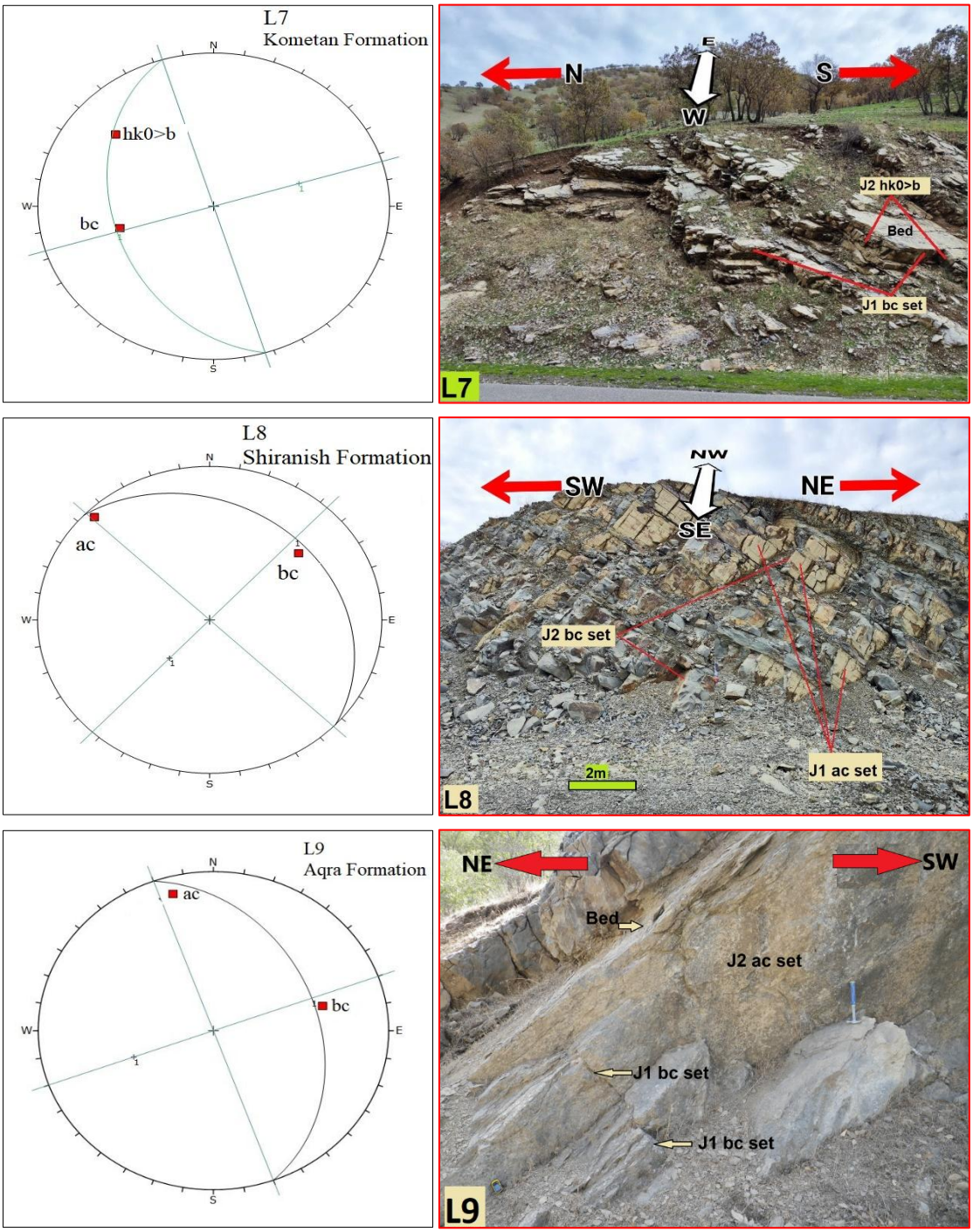

Figure 9. Shows stereographic projection of the joints and field photos of (L7, L8, and L9) stations.

8.2. Landslide Frequency Ratio LFR

The FR was calculated by dividing the landslide occurrence ratio by the area ratio for each class of each landslide conditioning (causative) factor. Table (5) reveals that the total area and pixels of an observed landslide that was used as input for creating a landslide frequency ratio susceptibility map (LFR) is 110312.5 m^2 (706) pixels. The six parameters which are slope, curvature, distance to road, distance to stream, aspect, and topography integrated into the

ArcGIS tool and classified based on statistical approaches for predicting the hazard zones within the study area. Finally, the LSM was created as in Figure (10), and its map shows five different classes which are very low, low, moderate, high, and very high as shown in (Table 6). The area of each class was determined based on pixel numbers in each class using statistical tools in ArcGIS software. The highest frequency is the moderate class which covers 34.6 Km^2 of the total study area while the lowest frequency class is high hazard which covers only 5.5 percent of the study area as shown in (Table 6).

Table 5. Calculation of the FR for slope, curvature, distance to road, distance to stream, aspect, and topography.

Parameter	classes	class pixels	%class pixels	Landslide pixels	%Landslide pixels	Frequency ratio	Area	Rf (relative frequency)	Rf (non)%	Rf (INT)
Slope	<10	154386	19.602	67	9.490	0.00043	0.00006	0.096	9.64	9.00
	10.1˚-20˚	161853	20.550	92	13.031	0.00057	0.00008	0.126	12.63	12
	20.1˚-30˚	189008	23.998	241	34.136	0.00128	0.00018	0.283	28.33	28
	30.1˚-40˚	194527	24.699	202	28.612	0.00104	0.00015	0.231	23.08	23
	>40.1˚	87819	11.150	104	14.731	0.00118	0.00017	0.263	26.32	26
	Total	787593		706		0.00450				
Curvature	Convex	377280	47.686	323	45.751	0.00087	0.00086	0.308	30.78	30
	Liner slope	11762	1.487	12	1.700	0.00102	0.00102	0.361	36.12	36
	Concave	402139	50.828	371	52.550	0.00094	0.00092	0.331	33.10	33
	Total	791181		706		0.00282				
Distance to road	>10	4409	6.000	92	13.031	0.02087	0.02087	0.541	54.07	54
	10.1-50	34761	47.305	450	63.739	0.01295	0.01295	0.335	33.55	33
	50.1-100	34313	46.695	164	23.229	0.00478	0.00478	0.124	12.38	12
	Total	73483		706		0.03859	0.00961			
Distance to Stream	>300	184728	23.660	428	60.623	0.00232	0.00232	0.547	54.73	54.00
	300.1-600	178485	22.860	148	20.963	0.00083	0.00083	0.195	19.59	19
	600.1-900	264320	33.854	64	9.065	0.00024	0.00024	0.0571	5.72	5
	900.1-1200	87081	11.153	42	5.949	0.00048	0.00048	0.113	11.39	11
	>1200	66138	8.471	24	3.399	0.00036	0.00036	0.085	8.57	8
	Total	780752		706		0.00423				
Aspect	Flat	5	0.001	0	0.000	0.00000	0.00000	0.000	0.00	0.00
	North	49844	6.329	13	1.841	0.00026	0.00026	0.032	3.21	3.00
	Northeast	126590	16.073	74	10.482	0.00058	0.00058	0.072	7.19	7.00
	East	121120	15.379	117	16.572	0.00097	0.00097	0.119	11.87	11.00
	Southeast	79914	10.147	16	2.266	0.00020	0.00020	0.025	2.46	2.00
	South	74880	9.507	3	0.425	0.00004	0.00004	0.005	0.49	1.00
	Southwest	117456	14.913	31	4.391	0.00026	0.00026	0.032	3.24	3.00
	West	180458	22.913	296	41.926	0.00164	0.00164	0.202	20.16	20.00
	Northwest	37326	4.739	156	22.096	0.00418	0.00418	0.514	51.37	51.00
	Total	787593		706		0.00814				
Topography	>1050	49547	6.262	174	24.646	0.00351	0.00351	0.642	64.23	64.00
	1050.1-1250	385034	48.666	282	39.943	0.00073	0.00073	0.134	13.40	13.00
	1250.1-1450	248009	31.347	219	31.020	0.00088	0.00088	0.162	16.15	16.00
	1450.1-1650	91106	11.515	31	4.391	0.00034	0.00034	0.062	6.22	6.00
	1650.1-1850	17485	2.210	0	0.000	0.00000	0.00000	0.000	0.00	0.00
	Total	791181		706		0.00547				

Table 6. Coverage area of each class with Landside susceptibility map based on LFR.

Classes	OBJECTID *	Value	Pixels class	Class Area m^2	Class area Km^2	Class percent
Very low	1	1	141627	22129220	22.1	18.1
Low	2	2	204743	31991090	32.0	26.2
Moderate	3	3	270491	42264220	42.3	34.6
High	4	4	120990	18904690	18.9	15.5
Very high	5	5	42903	6703594	6.7	5.5
			780754		122.0	100
Total			total Pixels		Class Area	

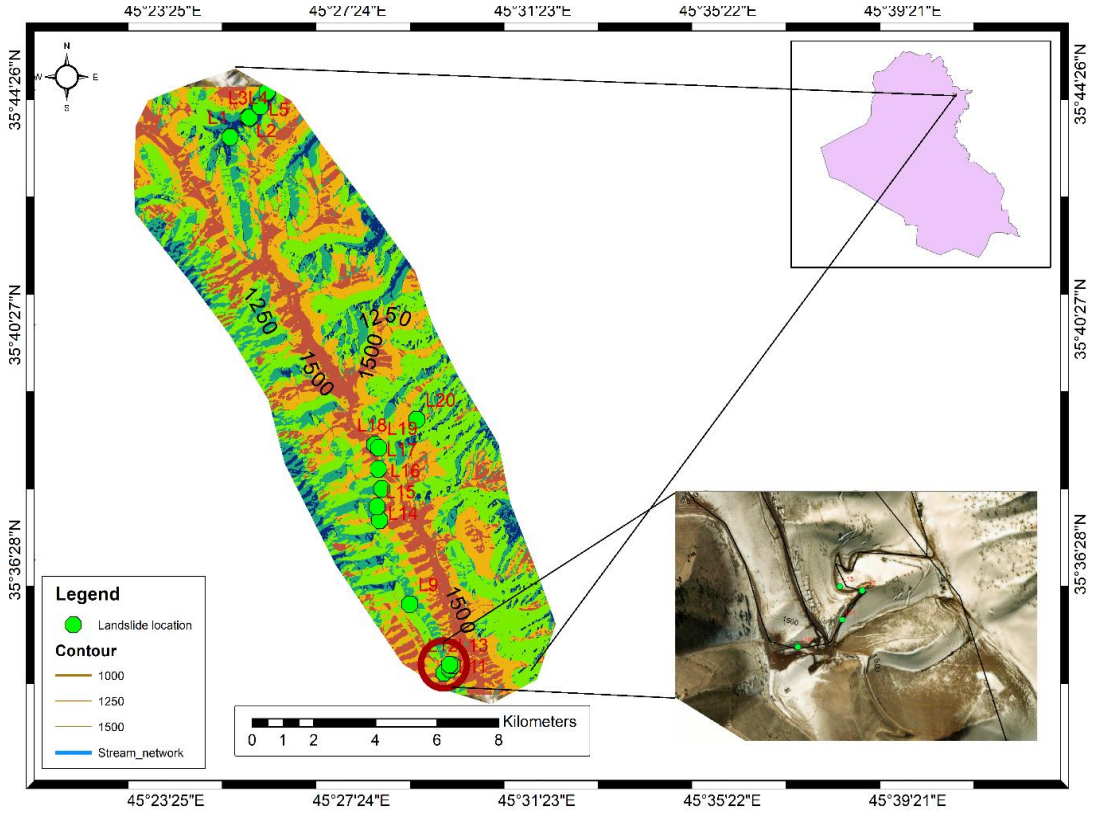

Figure 10. Shows landslide susceptibility zones.

8.3. Analytical Hierarchy Process

Using six important parameters in the study area landslide susceptibility map is created, and the weights and ranks of the factors and their contribution are represented in (Tables 7 and 8). These weights show the importance of each criterion in LSM (Figure 11), Also it demonstrates the influence of the selected parameters. It is a clear slope that has a great effect followed by Slope, Curvature, Aspect, Elevation, distance to road, and distance to stream, respectively.

The weighting of criteria was done based on field observation, and which of the parameters will be more significant for occurring landslides and cause more risks than others. The LSM model is classified into five classes (very low, low, moderate, high, and very high) according to natural breaks and intervals (Figure 12). In this regard, the result shows the study area contains five different zones including very low, moderate, high, and very high,), respectively (Figure 13), and the area of each class was calculated as shown in (Table 9).

Table 7. Pair-wise comparison of influencing parameters.

	1	**2**	**3**	**4**	**5**	**6**
Slope 1	**1**					
Curvature 2	0.333	**1**				
D- Road 3	0.25	0.5	**1**			
D- Stream 4	0.25	0.5	1	**1**		
Aspect 5	0.5	1	2	2	**1**	
Elevation 6	0.5	1	2	2	1	**1**

Table 8. Calculated weight of the parameters and their class descriptions.

Parameter	**classes**	**Rank**	**Description**	**Weight ofParameters**
Slope	<10	1	No Hazard	35.4
	10.1˚-20˚	2	V. Low	
	20.1˚-30˚	3	Moderate	
	30.1˚-40˚	4	High	
	>40.1˚	5	V. High	
Curvature	Convex	5	V. High	15.4
	Liner slope	2	Low	
	Concave	3	Moderate	
Distance to road	<10	5	V. High	8.2
	10.1-50	3	Moderate	
	50.1-100	2	Low	
Distance to Stream	<300	5	V. High	8.2
	300.1-600	3	Moderate	
	600.1-900	2	Low	
	900.1-1200	1	No hazard	
	>1200	1	No Hazard	
Aspect	Flat	1	No Hazard	16.4
	North	3	Moderate	
	Northeast	5	V. High	
	East	2	Low	
	Southeast	2	Low	
	South	2	Low	
	Southwest	5	V. High	
	West	3	Moderate	
	Northwest	3	Moderate	
Topography	<1050	2	Low	16.4
	1050.1-1250	3	Moderate	
	1250.1-1450	4	High	
	1450.1-1650	5	V. High	
	1650.1-1850	3	Moderate	

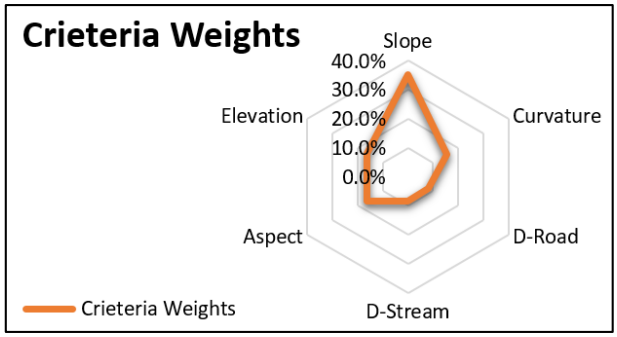

Figure 11. Radar map shows the weight importance of the parameters in the area.

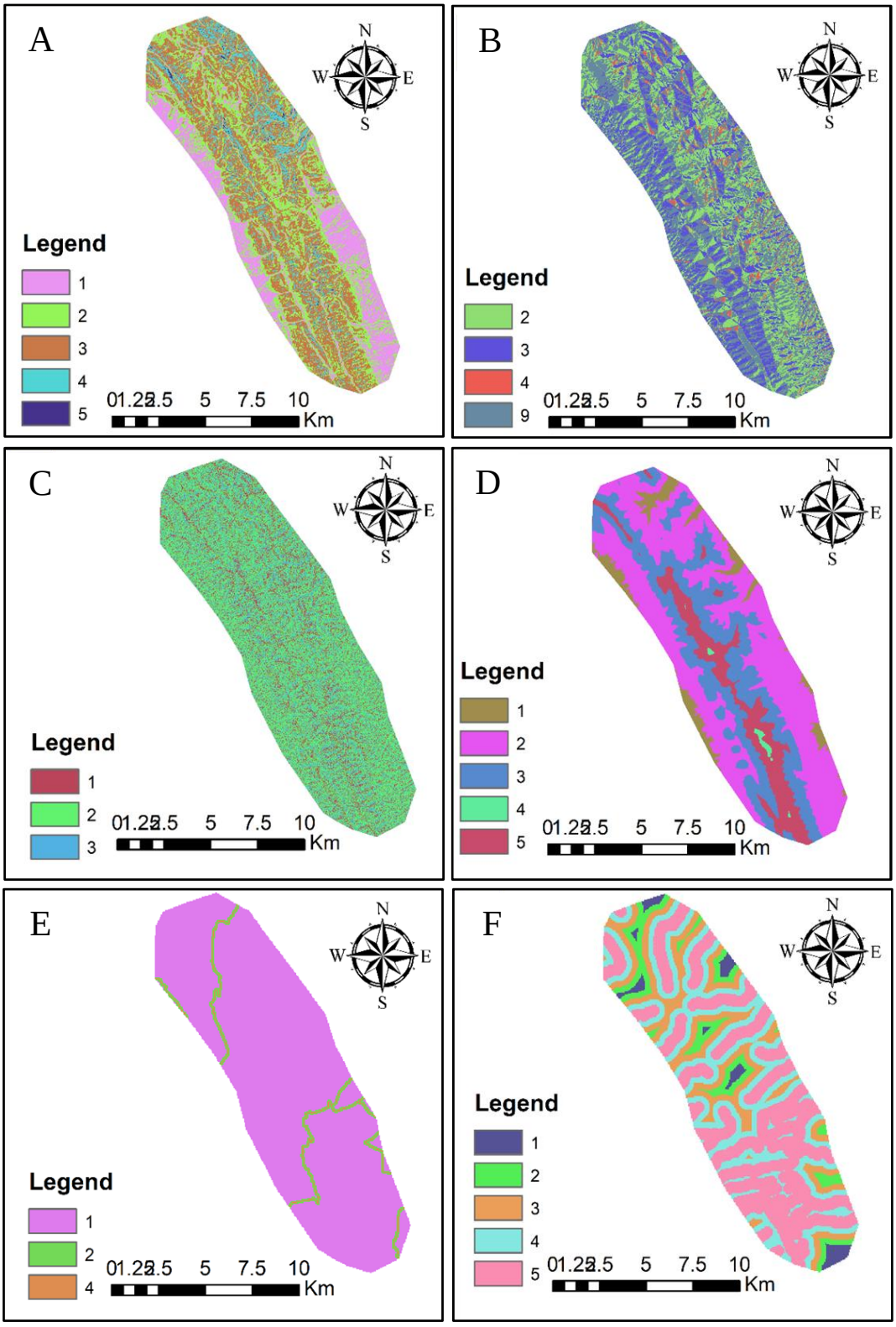

Figure 12. Reclassified maps of the selected parameters A) reclassified slop, B) reclassified aspect, C) reclassified curvature, D) reclassified elevation, and E) reclassified distance to road Reclassified distance to stream.

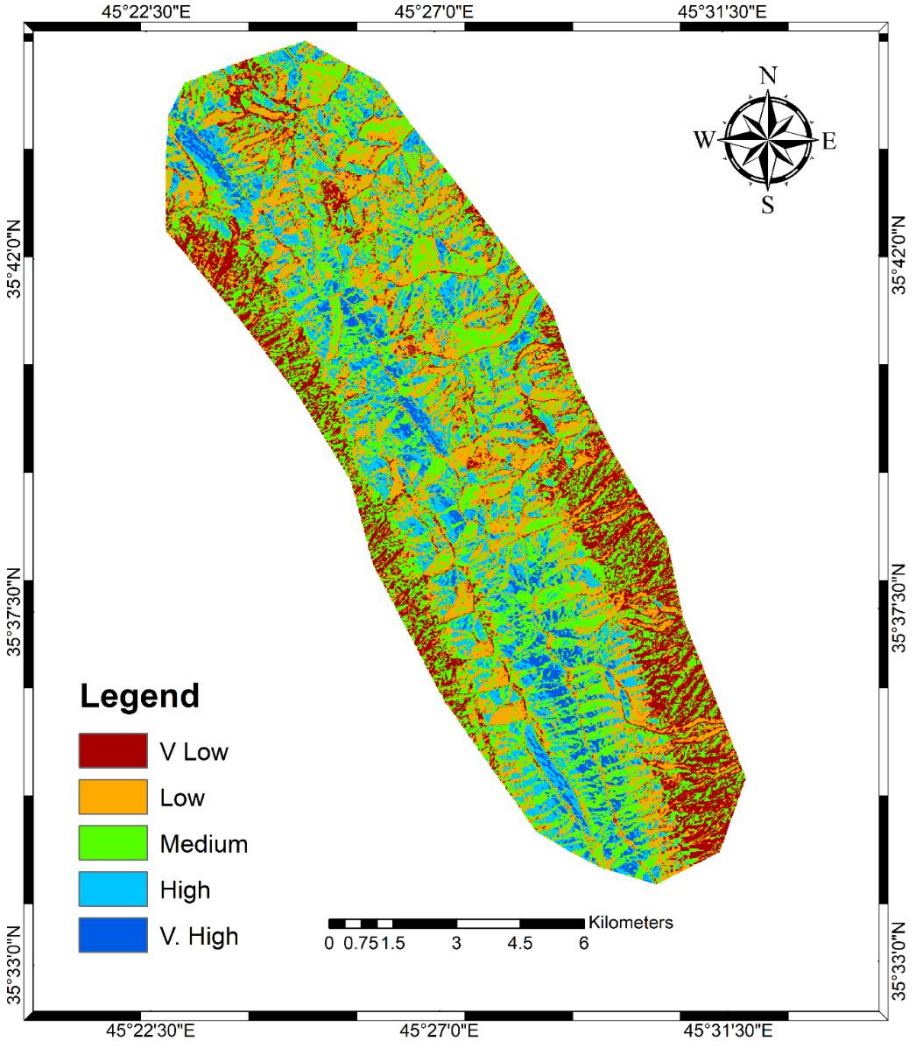

Figure 13. Landslide susceptibility map result of AHP technique.

Table 9. Coverage area of each class with landslide susceptibility map based on the AHP model.

Class percent	Class area Km^2	Class Area m^2	Pixels class	Value	OBJECTID	Classes
17.25	22.1	21,044,062	134682	1	1	Very Low
27.3	32.0	33,339,687	213374	2	2	Low
34.1	42.3	41,606,718	266283	3	3	Moderate
15.7	18.9	19,179,062	122746	4	4	High
5.6	6.7	6,823,281	43669	5	5	Very High
100	122.0		780754			
	Class Area		Total Pixels			Total

9. Discussion

For validation of LSM twenty stations were used for determining map accuracy of the study (Figure 14). The LSF and AHP models give 74% accuracy as shown in (Table 10). The resulting map was correlated with site data and field photos to check whether this model gave better predictions for an accessible area or for surveying large study areas. The accuracy of some

hazard zones gave giving very preferable result because some classes show high accuracy and are not mixed with other classes except some low classes, but these classes were mixed with other classes because of the pixel size which is (12.5×12.5 m) as shown in (Table 10).

Table 10. Accuracy assessment matrix for ground truth and model results.

LSD Susceptibility Map		Ground truth						
	Classes	Very low	Low	Moderate	High	Very high	Total	Accuracy
	Very low	0	0	0	0	0	0	0
	Low	0	4	1	0	0	5	%80
	Moderate	0	2	6	2	0	10	%60
	High	0	0	0	4	0	4	%100
	Very High	0	0	0	0	0	0	0
	Total	0	6	7	6	0	19	
	Accuracy	0	50 %	85%	50 %	0		

Overall accuracy (OA; Equation 3) determines the proportion of sites that have been correctly mapped. It is obtained by dividing the total number of pixels that are correctly classified by the total number of pixels. The OA is 73.8 %.

$$OA = \frac{\text{Total number of correctly classified pixels(14)}}{\text{Total number of reference pixels(19)}} * 100 = 73.8\%$$

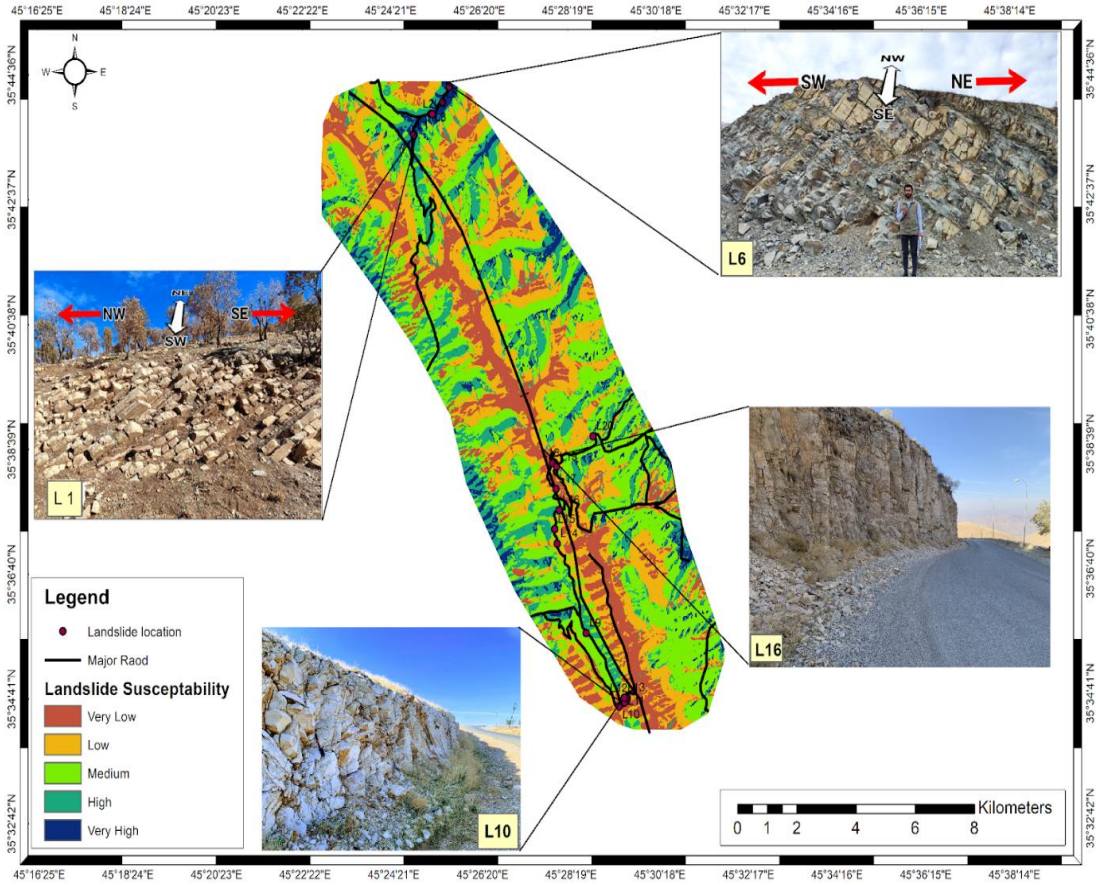

Figure 14. Landslide susceptibility mapping with field verification sites.

5. Conclusions

This study evaluated the risk of landslides along a network of roads that cross the steep mountain series of Qaiwan, Goizha, and Azmer in North Iraq. Previous roadside slope failures have demonstrated the serious risk posed by these slopes, especially in the winter and spring. Structural analysis of discontinuity reveals that the ac and bc set with hk0 > a, hk0 > b, and h0l > c systems are the most dominant discontinuity which acts as back, lateral, and basal release surfaces, also cause the occurrence of different types of landslide from more to less are wedge sliding, toppling, plane sliding, and rockfall. Two techniques were used in the paper to assess landslip vulnerability and create a hazard map. The first is the Landslide Frequency Ratio (LFR), which divides the region into five hazard zones: very low, low, moderate, high, and very high by combining six thematic maps (slope, aspect, curvature, topography, stream distance, and road distance) with historical landslide occurrences. The moderate hazard zone was the most extensive, covering 42 Km². The second one is the Analytical Hierarchy Process (AHP): Similar to LFR, AHP assigned weights to various factors (slope, curvature, aspect, distances to roads and streams, and topography) and resulted in the same five hazard zones, with moderate being the most prevalent. The validation process for AHP and LFR models was done using nineteen points and yielded an overall accuracy of 73.8%, with the highest accuracy in the moderate hazard class. This suggests that most unstable slopes fall within this zone, aligning with the results from both hazard maps and kinematic analysis. Landslide hazard assessment is a valuable tool for authorities to manage traffic safety. By identifying high-hazard areas (covering 42 Km² in this case), they can implement mitigation strategies such as slope stabilization and traffic signs.

Acknowledgment

The authors are grateful to Dr. Ghafor Ameen Hamasur from the University of Sulaimani for valuable comments that helped to improve the quality of this paper.

References

Abedini, M., & Tulabi, S. (2018). Assessing LNRF, FR, and AHP models in landslide susceptibility mapping index: A comparative study of Nojian watershed in Lorestan province, Iran. *Environmental Earth Sciences, 77*(11), 405. https://doi.org/10.1007/s12665-018-7524-1

Achour, Y., Boumezbeur, A., Hadji, R., Chouabbi, A., Cavaleiro, V., & Bendaoud, E. A. (2017). Landslide susceptibility mapping using analytic hierarchy process and information value methods along a highway road section in Constantine, Algeria. *Arabian Journal of Geosciences, 10*(8), 194. https://doi.org/10.1007/s12517-017-2980-6

Alavi, M. (2007). Structures of the Zagros fold-thrust belt in Iran. *American Journal of Science*, *307*(9), 1064–1095.

Al-Hakary, S. H. (2011). *H. Geometrical analysis and structural evolution of a selected area from NE Zagros Fold Thrust Belt and their tectonic implications, Northeast Iraq region, NE Iraq*. Sulaimani.

Al-Jumaily, I. (2004). *Tectonic investigation of the brittle failure structures in the Foreland Folds Belt. Northern Iraq, Unpub*.

Arjmandzadeh, R., Sharifi Teshnizi, E., Rastegarnia, A., Golian, M., Jabbari, P., Shamsi, H., & Tavasoli, S. (2020). GIS-Based Landslide Susceptibility Mapping in Qazvin Province of Iran. *Iranian Journal of Science and Technology, Transactions of Civil Engineering, 44*(S1), 619–647. https://doi.org/10.1007/s40996-019-00326-3

Basharat, M., Shah, H. R., & Hameed, N. (2016). Landslide susceptibility mapping using GIS and weighted overlay method: A case study from NW Himalayas, Pakistan. *Arabian Journal of Geosciences*, *9*(4), 292. https://doi.org/10.1007/s12517-016-2308-y

Buday, T. (1980). *The regional geology of Iraq: Stratigraphy and paleogeography* (Vol. 1). State Organization for Minerals, Directorate General for Geological Survey ….

Choi, J., Oh, H.-J., Lee, H.-J., Lee, C., & Lee, S. (2012). Combining landslide susceptibility maps obtained from frequency ratio, logistic regression, and artificial neural network models using ASTER images and GIS. *Engineering Geology*, *124*, 12–23.

Das, I., Stein, A., Kerle, N., & Dadhwal, V. K. (2012). Landslide susceptibility mapping along road corridors in the Indian Himalayas using Bayesian logistic regression models. *Geomorphology*, *179*, 116–125.

El Jazouli, A., Barakat, A., & Khellouk, R. (2019). GIS-multicriteria evaluation using AHP for landslide susceptibility mapping in Oum Er Rbia high basin (Morocco). *Geoenvironmental Disasters*, *6*(1), 3. https://doi.org/10.1186/s40677-019-0119-7

Feizizadeh, B., Roodposhti, M. S., Jankowski, P., & Blaschke, T. (2014). A GIS-based extended fuzzy multi-criteria evaluation for landslide susceptibility mapping. *Computers & Geosciences*, *73*, 208–221.

Fouad, S. F. (2015). Tectonic map of Iraq, scale 1: 1000 000, 2012. *Iraqi Bulletin of Geology and Mining*, *11*(1), 1–7.

Hamasur, G. A., & Qadir, N. M. (2020). Slope Stability Assessment along Qalachwalan-Suraqalat Main Road, Sulaimani, NE-Iraq. *Tikrit Journal of Pure Science*, *25*(3), 26–48.

Hancock, P. (1985). Brittle microtectonics: Principles and practice. *Journal of Structural Geology*, *7*(3–4), 437–457.

Hancock, P., & Atiya, M. (1979). Tectonic significance of mesofracture systems associated with the Lebanese segment of the Dead Sea transform fault. *Journal of Structural Geology*, *1*(2), 143–153.

Jaafari, A., Najafi, A., Pourghasemi, H., Rezaeian, J., & Sattarian, A. (2014). GIS-based frequency ratio and index of entropy models for landslide susceptibility assessment in the Caspian forest, northern Iran. *International Journal of Environmental Science and Technology*, *11*, 909–926.

Jassim, S. Z., & Goff, J. C. (2006). *Geology of Iraq*. DOLIN, sro, distributed by Geological Society of London.

Lee, S., Lee, S., Lee, M.-J., & Jung, H.-S. (2018). Spatial assessment of urban flood susceptibility using data mining and geographic information System (GIS) tools. *Sustainability*, *10*(3), 648.

Lee, S., & Pradhan, B. (2007). Landslide hazard mapping at Selangor, Malaysia using frequency ratio and logistic regression models. *Landslides*, *4*(1), 33–41.

Mamlesi, F. (2010). Engineering geological study of rock slope stability along the Dokan-Khalakan road, Kurdistan Region, NE-Iraq. *Unpublished M. Sc. Thesis, University of Sulaimani, Sulaimani. Sulaimani, Iraq: University of Sulaimani*.

Mohammad, F. O. (2023). *Engineering geological assessment of proposed goma-qazan dam site within Kanarwe rive sub basin and its hydrological conditions Sulaymaniyah-NE Iraq* [Unpublished]. http://dx.doi.org/10.13140/RG.2.2.11900.76165

Mohammed, F. O., Ahmed, A. J., & Mohammed, S. H. (2020). Landslide susceptibility assessment along Biyara-Tawella road, Kurdistan region, NE-Iraq. *Zankoy*, *22*(1), 1–38.

Nefeslioglu, H. A., Gokceoglu, C., & Sonmez, H. (2008). An assessment on the use of logistic regression and artificial neural networks with different sampling strategies for the preparation of landslide susceptibility maps. *Engineering Geology*, *97*(3–4), 171–191.

Park, S., Choi, C., Kim, B., & Kim, J. (2013). Landslide susceptibility mapping using frequency ratio, analytic hierarchy process, logistic regression, and artificial neural network methods at the Inje area, Korea. *Environmental Earth Sciences*, *68*, 1443–1464.

Ramsay, J. G., Huber, M. I., & Lisle, R. J. (1983). *The techniques of modern structural geology: Folds and fractures* (Vol. 2). Academic Press.

Saaty, T. (1980). *The analytic hierarchy process (AHP) for decision making*. *1*, 69.

Saaty, T. L. (2008). Decision making with the analytic hierarchy process. *International Journal of Services Sciences*, *1*(1), 83–98.

Saaty, T. L., Vargas, L. G., Saaty, T. L., & Vargas, L. G. (2012). The seven pillars of the analytic hierarchy process. *Models, Methods, Concepts & Applications of the Analytic Hierarchy Process*, 23–40.

Saranaathan, S., Mani, S., Ramesh, V., & Prasanna Venkatesh, S. (2021). Landslide susceptibility zonation mapping using bivariate statistical frequency ratio method and GIS: a case study in part of SH 37 Ghat Road, Nadugani, Panthalur Taluk, The Nilgiris. *Journal of the Indian Society of Remote Sensing*, *49*, 275–291.

Sarkar, S., & Kanungo, D. (2004). An integrated approach for landslide susceptibility mapping using remote sensing and GIS. *Photogrammetric Engineering & Remote Sensing*, *70*(5), 617–625.

Tesfa, C. (2022). GIS-Based AHP and FR Methods for Landslide Susceptibility Mapping in the Abay Gorge, Dejen–Renaissance Bridge, Central, Ethiopia. *Geotechnical and Geological Engineering*, *40*(10), 5029–5043. https://doi.org/10.1007/s10706-022-02197-4

Turner, F. J., & Weiss, L. E. (1963). Structural analysis of metamorphic tectonics. *(No Title)*.

Wind, Y., & Saaty, T. L. (1980). Marketing applications of the analytic hierarchy process. *Management Science*, *26*(7), 641–658.

Wu, Y., Li, W., Liu, P., Bai, H., Wang, Q., He, J., Liu, Y., & Sun, S. (2016). Application of analytic hierarchy process model for landslide susceptibility mapping in the Gangu County, Gansu Province, China. *Environmental Earth Sciences*, *75*(5), 422. https://doi.org/10.1007/s12665-015-5194-9

Yalcin, A. (2008). GIS-based landslide susceptibility mapping using analytical hierarchy process and bivariate statistics in Ardesen (Turkey): Comparisons of results and confirmations. *CATENA*, *72*(1), 1–12. https://doi.org/10.1016/j.catena.2007.01.003

About the authors

Dr. Fahmy Osman Mohammed began his academic journey at the University of Sulaimani, earning a Bachelor of Science in Geology in 2005. He continued his studies there, specializing in Engineering Geology with a Master's degree in 2011. Most recently, in 2023, he completed his Ph.D. within the Geology Department at the same university. Dr. Mohammed brings 15 years of experience to the fields of Engineering Geology, Environmental Modeling, Remote Sensing, and GIS. His expertise is further demonstrated by his ten published articles on various geological topics.

e-mail: fahmy.mohammed@univsul.edu.iq

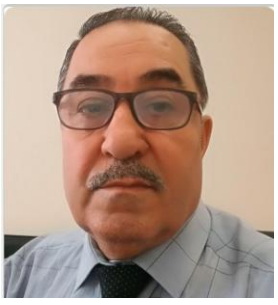

Dr. Salim Hasan Suleiman Al-Hakari earned a bachelor's degree in 1989 and a master's degree in 1993, both from the University of Mosul, specializing in structural geology with a focus on paleo stress analysis. He began his academic career as a lecturer assistant at the University of Sulaimani in 2004. In 2011, he completed his Ph.D. at the same university, researching the geometry of folds around Sulaymaniyah City. Currently, he holds the position of professor in structural geology. His research contributions include eleven published papers on paleo stress analysis and fold geometry.

e-mail: salim.sulaiman@univsul.edu.iq

Ashna Jalal Ahmed is a Ph.D. student in engineering geology at the Department of Earth Science and Petroleum, University of Sulaimani, and the Institute of Water Resources and Environmental Management at the University of Miskolc. She earned her B.Sc. in Geology in 2010 from the University of Sulaimani and later completed her M.Sc. in Engineering Geology (Evaluation of Tunnel site investigation) at the University of Cairo, Egypt in 2017. From 2011-2015, Ashna worked as a demonstrator at the Department of Geology University of Sulaimani and continued as an assistant lecturer from 2018-2024. Currently, she is pursuing her Ph.D. research in dam site investigation.

e-mail: ashna.ahmed@univsul.edu.iq

Sarkhel Hawre Mohammed is a Ph.D. candidate in Water Resources Management at the Faculty of Earth Sciences and Environmental Sciences and Engineering, University of Miskolc, Hungary. He earned his B.Sc. in Geology in 2013 from the University of Sulaimani and later completed his M.Sc. in Hydrogeological Engineering at the University of Miskolc in 2017. From 2013 to 2015, Sarkhel served as a demonstrator in the Department of Geology at the University of Sulaimani and continued as an assistant lecturer from 2018 to 2022. Currently, he is pursuing his Ph.D. research in water resources management, with a focus on groundwater management and modeling.

e-mail: sarkhel.mohammed@univsul.edu.iq